

**Supplementary Information for:**

**PEGylation of an artificial O<sub>2</sub> and CO receptor: synthesis,  
characterisation and pharmacokinetic study**

**Takunori Ueda, Hiroaki Kitagishi and Koji Kano\***

Department of Molecular Chemistry and Biochemistry, Faculty of Science and  
Engineering, Doshisha University, Kyotanabe, Kyoto 610-0321, Japan.

**Table S1** Extinction coefficients of CO-coordinated hemoCD and PEG(mw)-hemoCDs at 422 nm in 0.05 M phosphate buffer at pH 7.0 and 25 °C.<sup>a</sup>

	$10^{-5} \epsilon_{422} / \text{M}^{-1} \text{cm}^{-1}$
hemoCD	3.71 <sup>b</sup>
PEG750-hemoCD	3.77
PEG5k-hemoCD	3.53
PEG10k-hemoCD	3.51
PEG20k-hemoCD	3.60

<sup>a</sup>CO-coordinated PEG(mw)-hemoCDs were quantitatively formed by the additions of excess  $\text{Na}_2\text{S}_2\text{O}_4$  to the solutions of the ferric-forms of PEG(mw)-hemoCDs under CO atmospheres. <sup>b</sup>Ref 35.

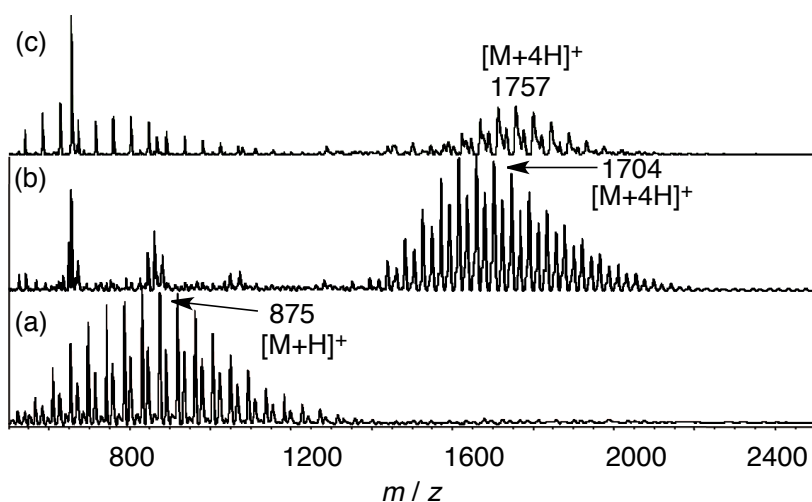


**Fig. S1** MALDI-TOF MS spectra of  $\text{HOOC}(\text{CH}_2)_3(\text{CO})\text{O-PEG750-OCH}_3$  (a, positive mode), P-PEG750 (b, negative mode) and  $\text{Fe}^{\text{III}}\text{P-PEG750}$  (c, negative mode) with a subsequent addition of a mixture of  $\alpha$ -cyano-4-hydroxycinnamic acid and 2,5-dihydroxybenzoic acid matrices.

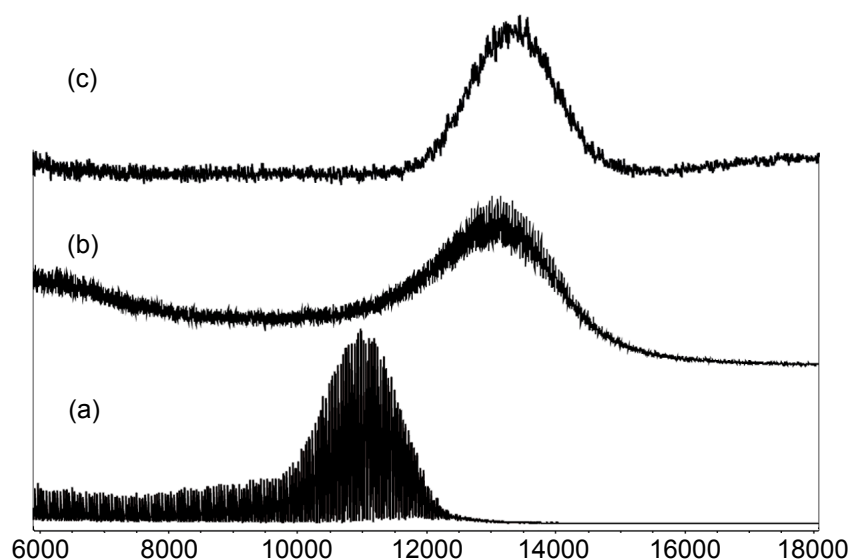


**Fig. S2** MALDI-TOF MS spectra of  $\text{HOOC}(\text{CH}_2)_3(\text{CO})\text{O-PEG10k-O}(\text{CO})(\text{CH}_2)_3\text{COOH}$  (a, positive mode), P-PEG10k (b, negative mode) and  $\text{Fe}^{\text{III}}\text{P-PEG10k}$  (c, negative mode) with a subsequent addition of a mixture of  $\alpha$ -cyano-4-hydroxycinnamic acid and 2,5-dihydroxybenzoic acid matrices.

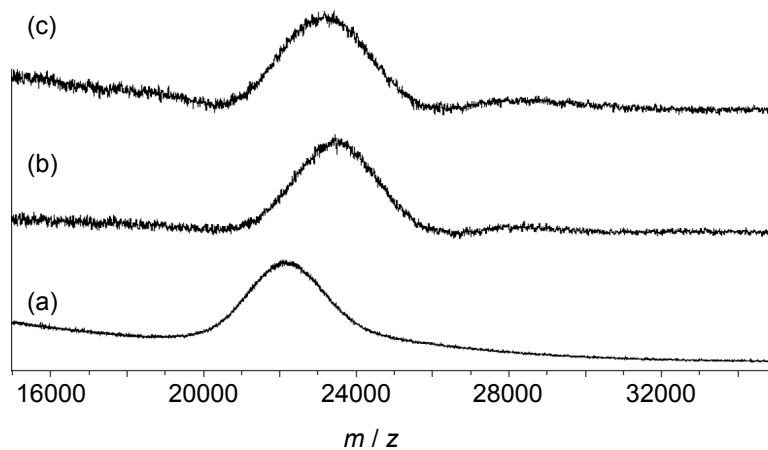


**Fig. S3** MALDI-TOF MS spectra of  $\text{HOOC}(\text{CH}_2)_3(\text{CO})\text{O-PEG20k-O}(\text{CO})(\text{CH}_2)_3\text{COOH}$  (a, positive mode), P-PEG20k (b, negative mode) and  $\text{Fe}^{\text{III}}\text{P-PEG20k}$  (c, negative mode) with a subsequent addition of a mixture of  $\alpha$ -cyano-4-hydroxycinnamic acid and 2,5-dihydroxybenzoic acid matrices.

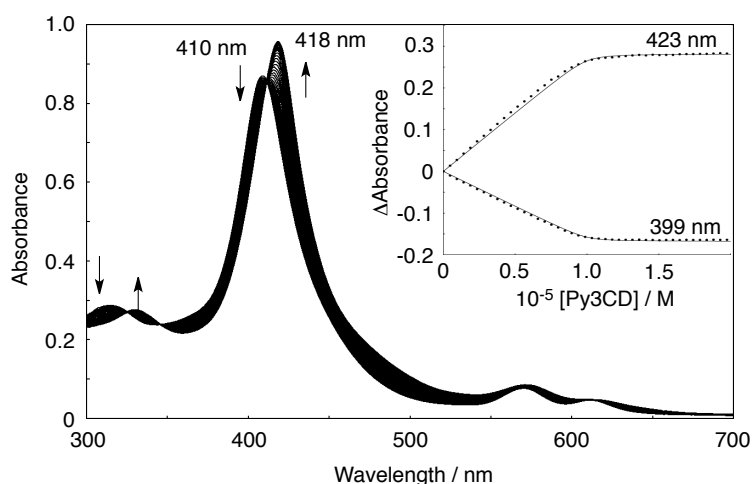


**Fig. S4** UV-Vis spectral changes of Fe<sup>III</sup>P-PEG750 (1 × 10<sup>-5</sup> M) upon addition of Py3CD in 0.05 M phosphate buffer at pH 7.0 and 25 °C. Inset shows plots of the changes in absorbances of Fe<sup>III</sup>P-PEG750 versus [Py3CD]. The solid lines indicate theoretical curves for the 1:1 complexation to give the binding constant (*K*).

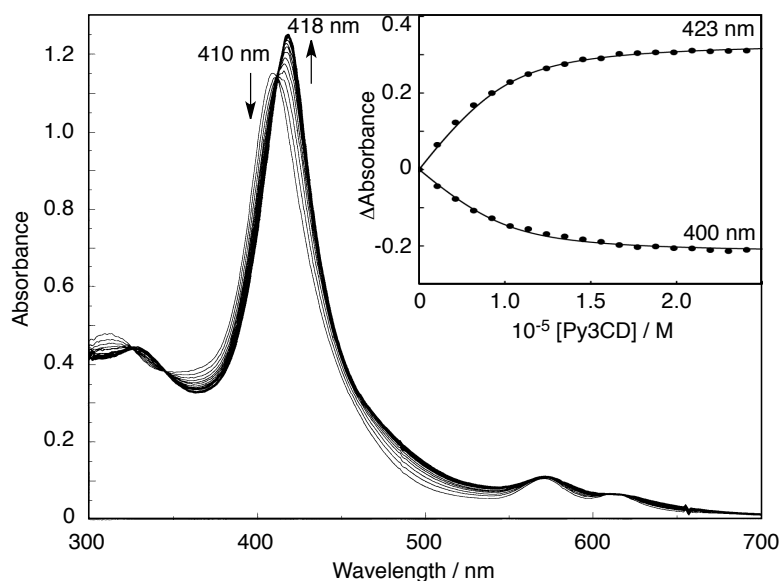


**Fig. S5** UV-Vis spectral changes of Fe<sup>III</sup>P-PEG10k (1 × 10<sup>-5</sup> M in the porphyrin concentration) upon addition of Py3CD in 0.05 M phosphate buffer at pH 7.0 and 25 °C. Inset shows plots of the changes in absorbances of Fe<sup>III</sup>P-PEG10k versus [Py3CD]. The solid lines indicate theoretical curves for the 1:1 complexation to give the binding constant (*K*).

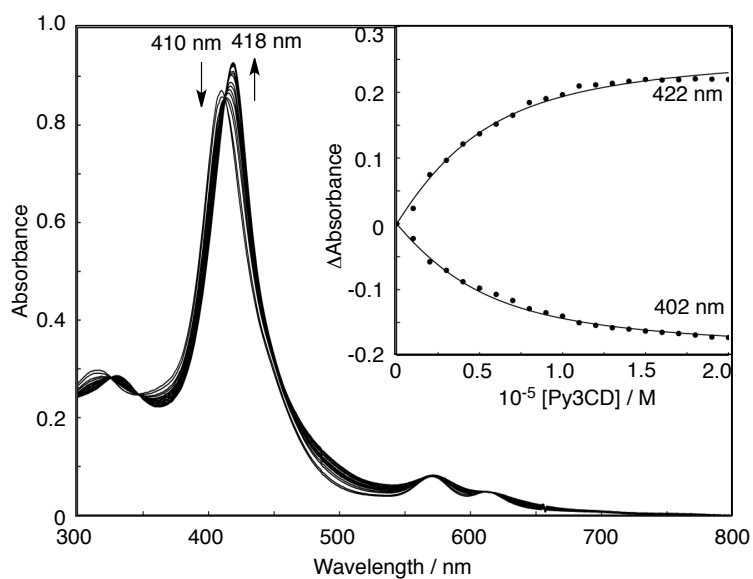
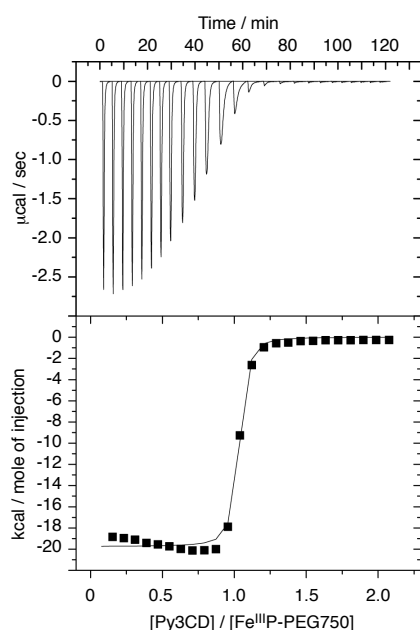
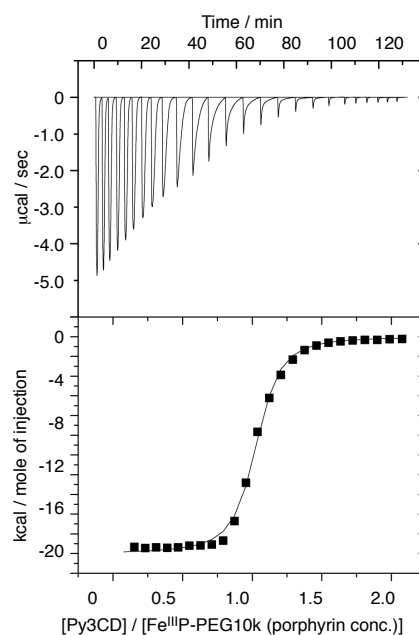


**Fig. S6** UV-Vis spectral changes of Fe<sup>III</sup>P-PEG20k (1 × 10<sup>-5</sup> M in the porphyrin concentration) upon addition of Py3CD in 0.05 M phosphate buffer at pH 7.0 and 25 °C. Inset shows plots of the changes in absorbances of Fe<sup>III</sup>P-PEG20k versus [Py3CD]. The solid lines indicate theoretical curves for the 1:1 complexation to give the binding constant ( $K$ ).

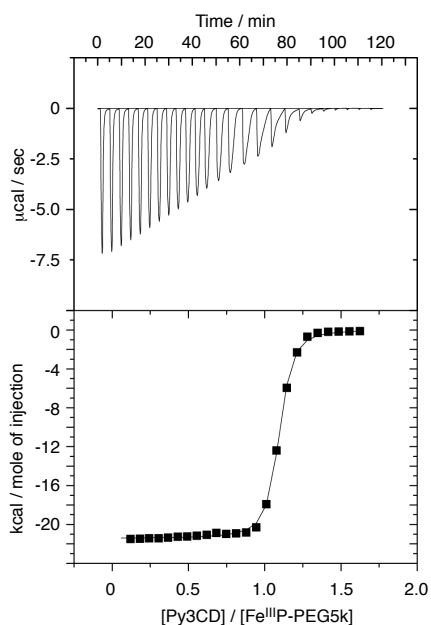
(a) cell : [Fe<sup>III</sup>P-PEG750] = 0.045 mM  
syringe : [Py3CD] = 0.5 mM  
(10  $\mu$ L x 25 injections)



(c) cell : [Fe<sup>III</sup>P-PEG10k] = 0.18 mM (porphyrin conc.)  
syringe : [Py3CD] = 2 mM  
(10  $\mu$ L x 25 injections)



(b) cell : [Fe<sup>III</sup>P-PEG5k] = 0.23 mM  
syringe : [Py3CD] = 2 mM  
(10  $\mu$ L x 25 injections)



(d) cell : [Fe<sup>III</sup>P-PEG20k] = 0.18 mM (porphyrin conc.)  
syringe : [Py3CD] = 2 mM  
(10  $\mu$ L x 25 injections)

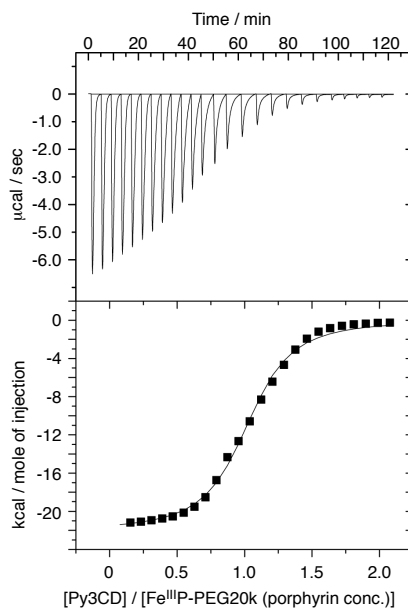


**Fig. S7** Calorimetric titrations of Fe<sup>III</sup>-PEG(mw)s with 25 aliquots (10  $\mu$ L each) of Py3CD in 0.05 M phosphate buffer at pH 7.0 and 298.15 K. The initial concentrations of Fe<sup>III</sup>-PEG(mw) in a cell and Py3CD in a syringe are given in the respective figures.

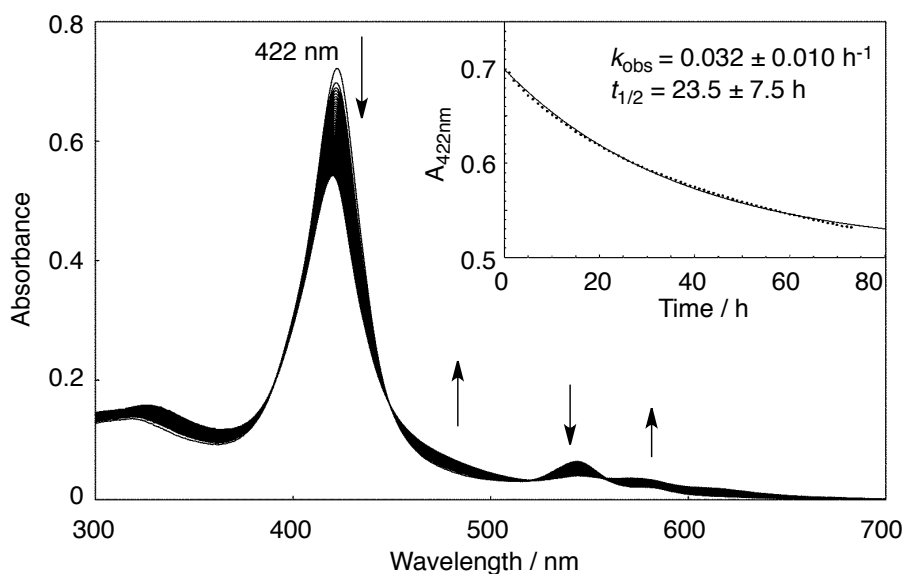


**Fig. S8** Autoxidation reaction of the O<sub>2</sub> adduct of PEG750-hemoCD ( $5.0 \times 10^{-6} \text{ M}$ ) under air in 0.05 M phosphate buffer at 25 °C. Scans were made at 1.0 hour intervals. Inset: First-order plot based on the absorption change at 422 nm.

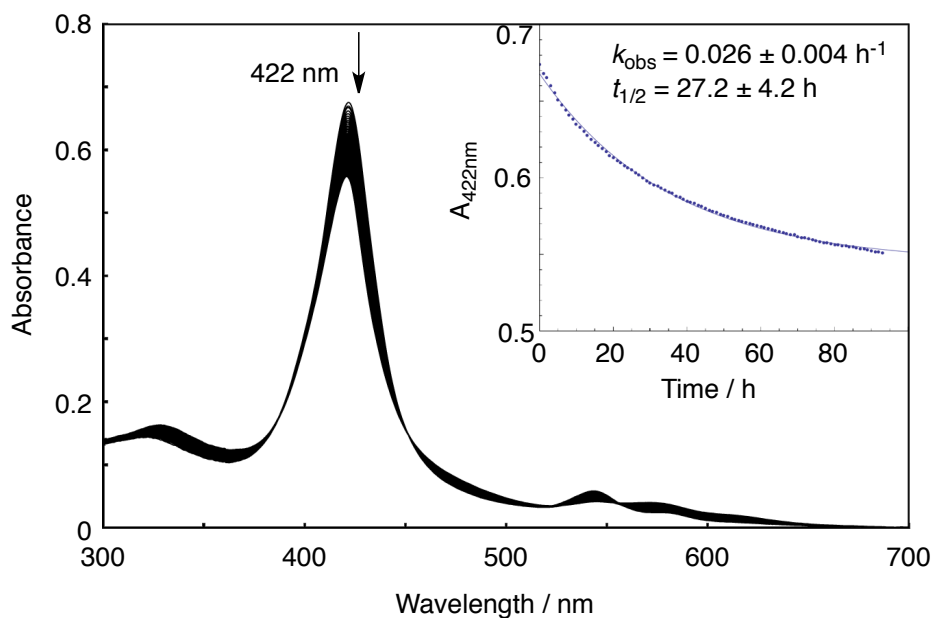


**Fig. S9** Autoxidation reaction of the O<sub>2</sub> adduct of PEG5k-hemoCD ( $5.0 \times 10^{-6} \text{ M}$ ) under air in 0.05 M phosphate buffer at 25 °C. Scans were made at 1.0 hour intervals. Inset: First-order plot based on the absorption change at 422 nm.

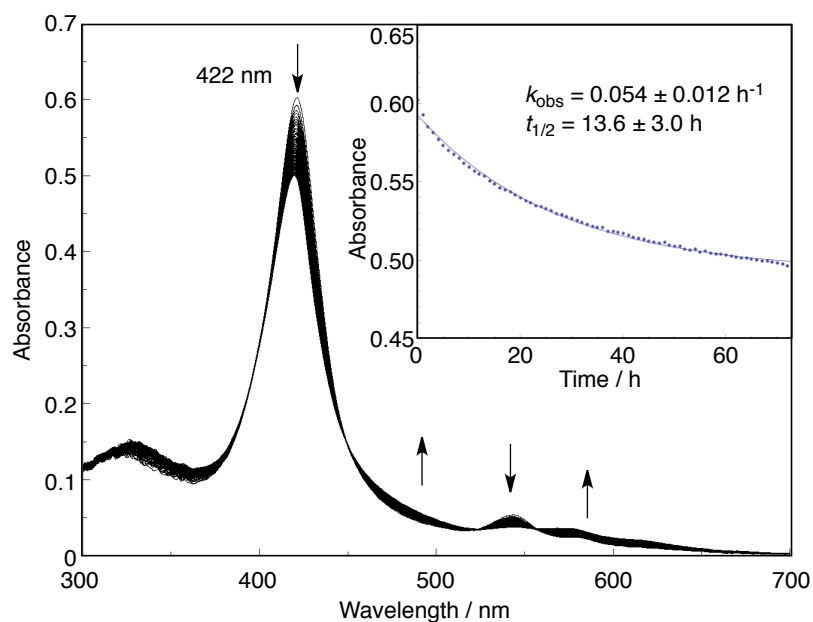


**Fig. S10** Autoxidation reaction of the O<sub>2</sub> adduct of PEG10k-hemoCD ( $5.0 \times 10^{-6} \text{ M}$ ) under air in 0.05 M phosphate buffer at 25 °C. Scans were made at 1.0 hour intervals. Inset: First-order plot based on the absorption change at 422 nm.

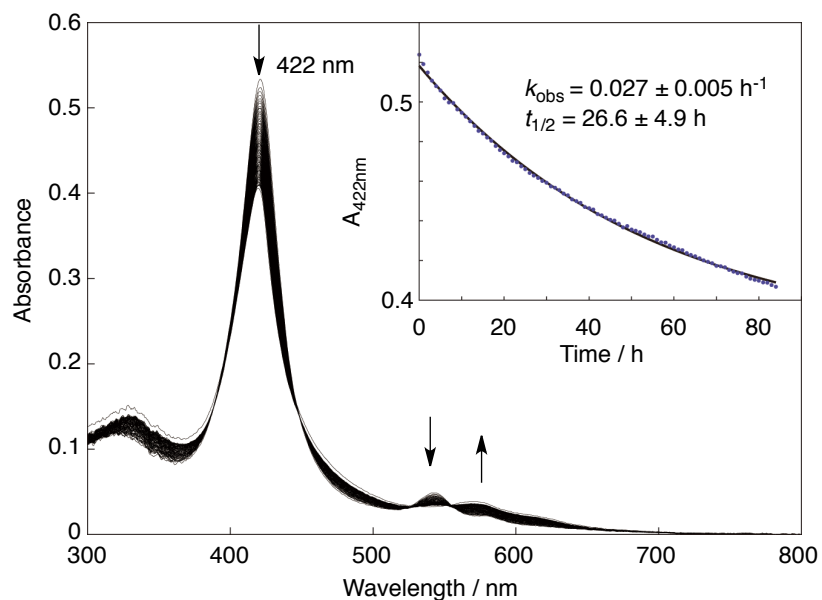


**Fig. S11** Autoxidation reaction of the O<sub>2</sub> adduct of PEG20k-hemoCD ( $5.0 \times 10^{-6} \text{ M}$ ) under air in 0.05 M phosphate buffer at 25 °C. Scans were made at 1.0 hour intervals. Inset: First-order plot based on the absorption change at 422 nm.



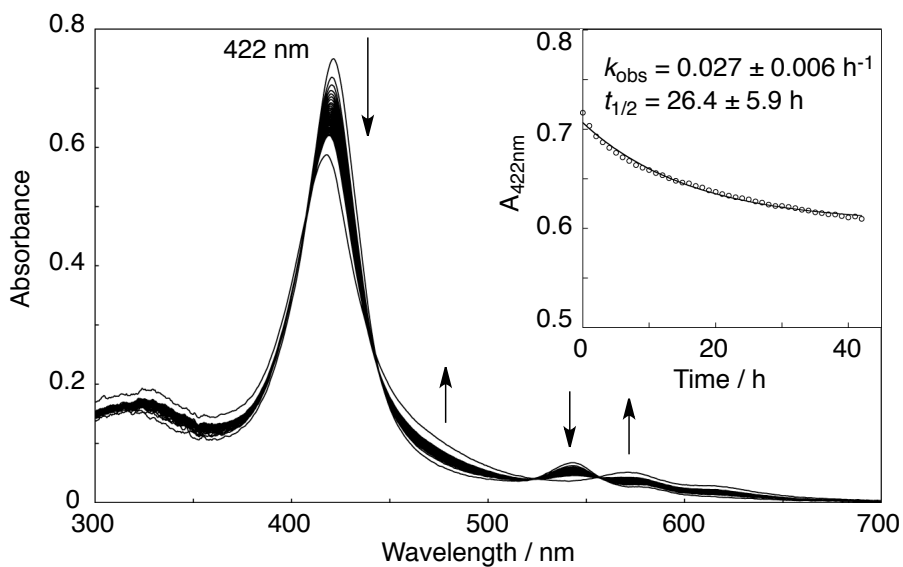


**Fig. S12** Autoxidation reaction of the O<sub>2</sub> adduct of PEG10k-hemoCD ( $5.0 \times 10^{-6} \text{ M}$ ) in the presence of catalase (100 units) under air in 0.05 M phosphate buffer at 25 °C. Scans were made at 1.0 hour intervals. Inset: First-order plot based on the absorption change at 422 nm.

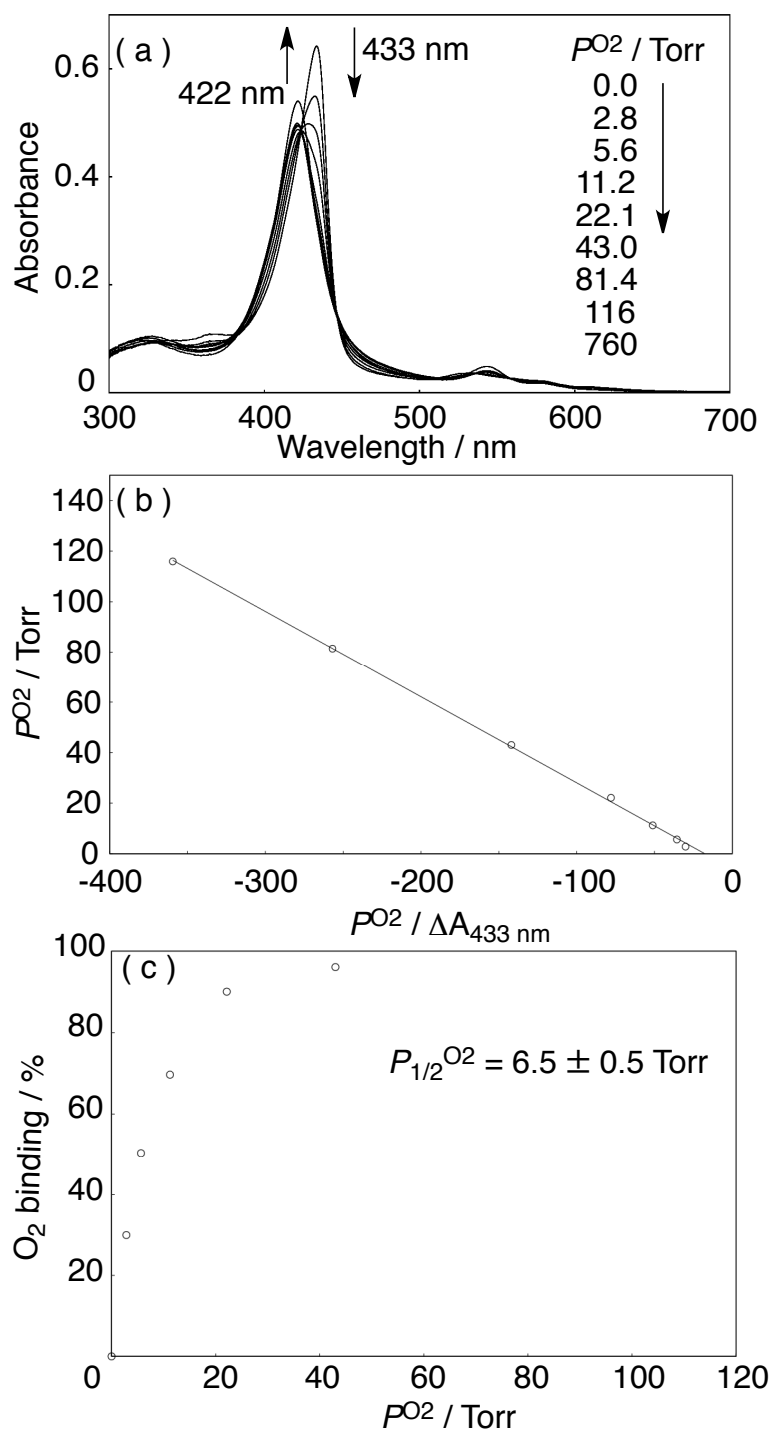


**Fig. S13** UV-Vis spectral changes of PEG750-hemoCD (5.0 x 10<sup>-6</sup> M) as a function of the O<sub>2</sub> partial pressure (P<sup>O<sub>2</sub></sup>) in N<sub>2</sub> in 0.05 M phosphate buffer at pH 7.0 and 25 °C (a), plot of P<sup>O<sub>2</sub></sup> / ΔA<sub>433 nm</sub> versus P<sup>O<sub>2</sub></sup> for determining P<sub>1/2</sub><sup>O<sub>2</sub></sup> (b) and the titration curve for O<sub>2</sub> binding to PEG750-hemoCD (c).

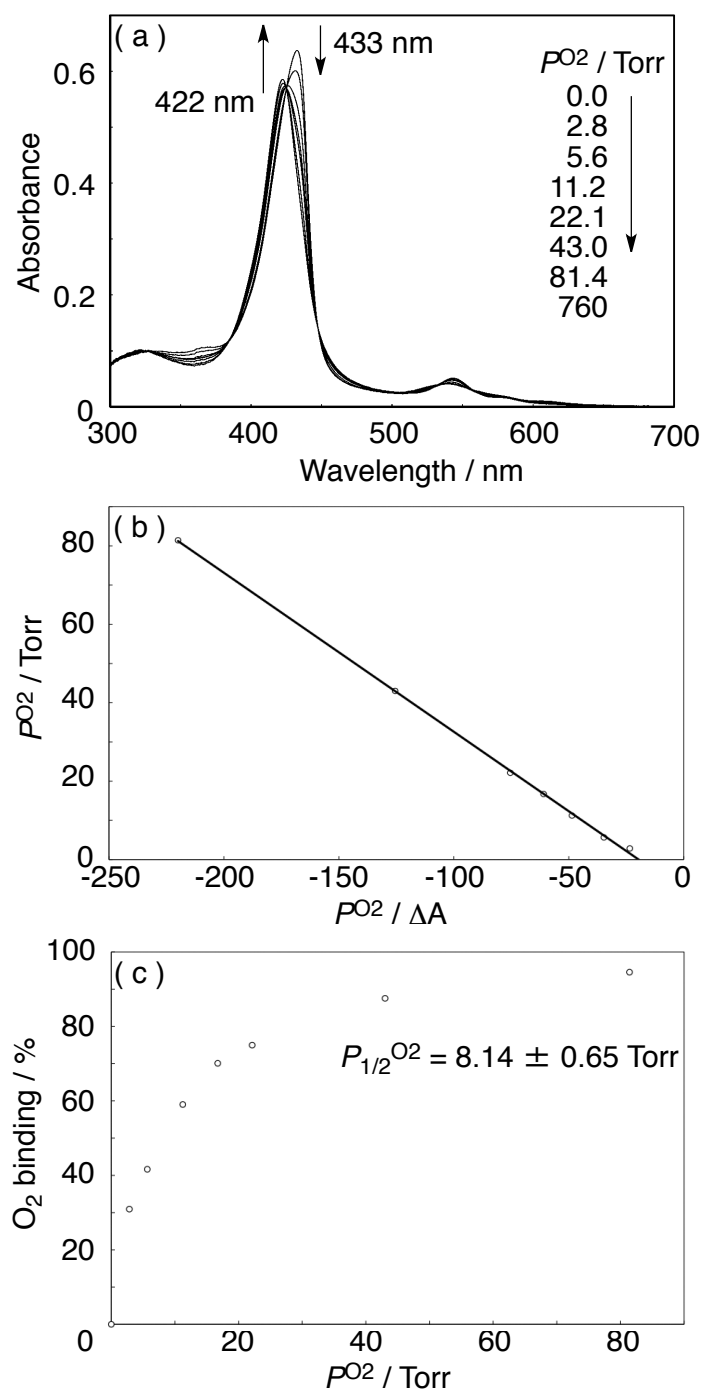


**Fig. S14** UV-Vis spectral changes of PEG5k-hemoCD (5.0 x 10<sup>-6</sup> M) as a function of the O<sub>2</sub> partial pressure ( $P^{O_2}$ ) in N<sub>2</sub> in 0.05 M phosphate buffer at pH 7.0 and 25 °C (a); plot of  $P^{O_2} / \Delta A_{433 \text{ nm}}$  versus  $P^{O_2}$  for determining  $P_{1/2}^{O_2}$  (b) and the titration curve for O<sub>2</sub> binding to PEG5k-hemoCD (c).

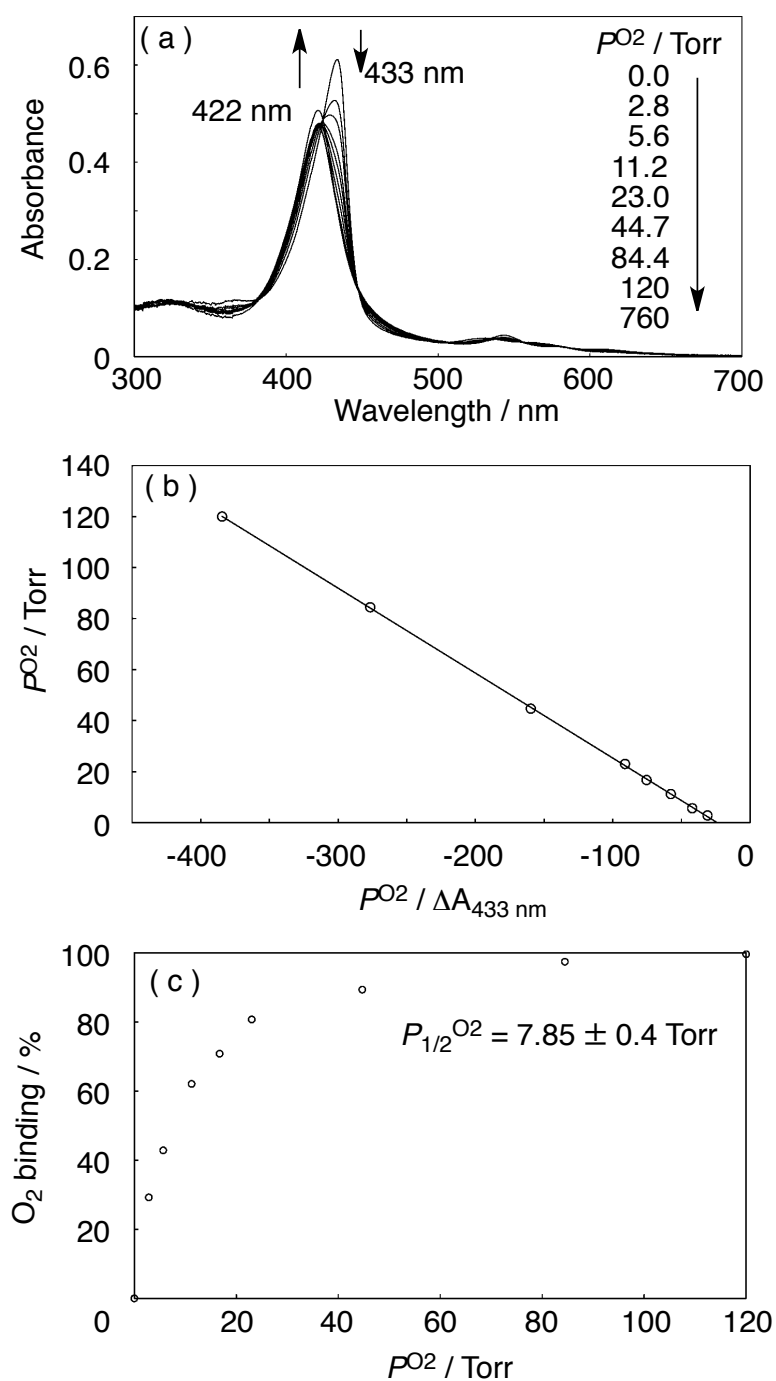


**Fig. S15** UV-Vis spectral changes of PEG10k-hemoCD ( $5.0 \times 10^{-6}$  M) as a function of the O<sub>2</sub> partial pressure ( $P^{O_2}$ ) in N<sub>2</sub> in 0.05 M phosphate buffer at pH 7.0 and 25 °C (a), plot of  $P^{O_2} / \Delta A_{433 \text{ nm}}$  versus  $P^{O_2}$  for determining  $P_{1/2}^{O_2}$  (b) and the titration curve for O<sub>2</sub> binding to PEG10k-hemoCD (c).

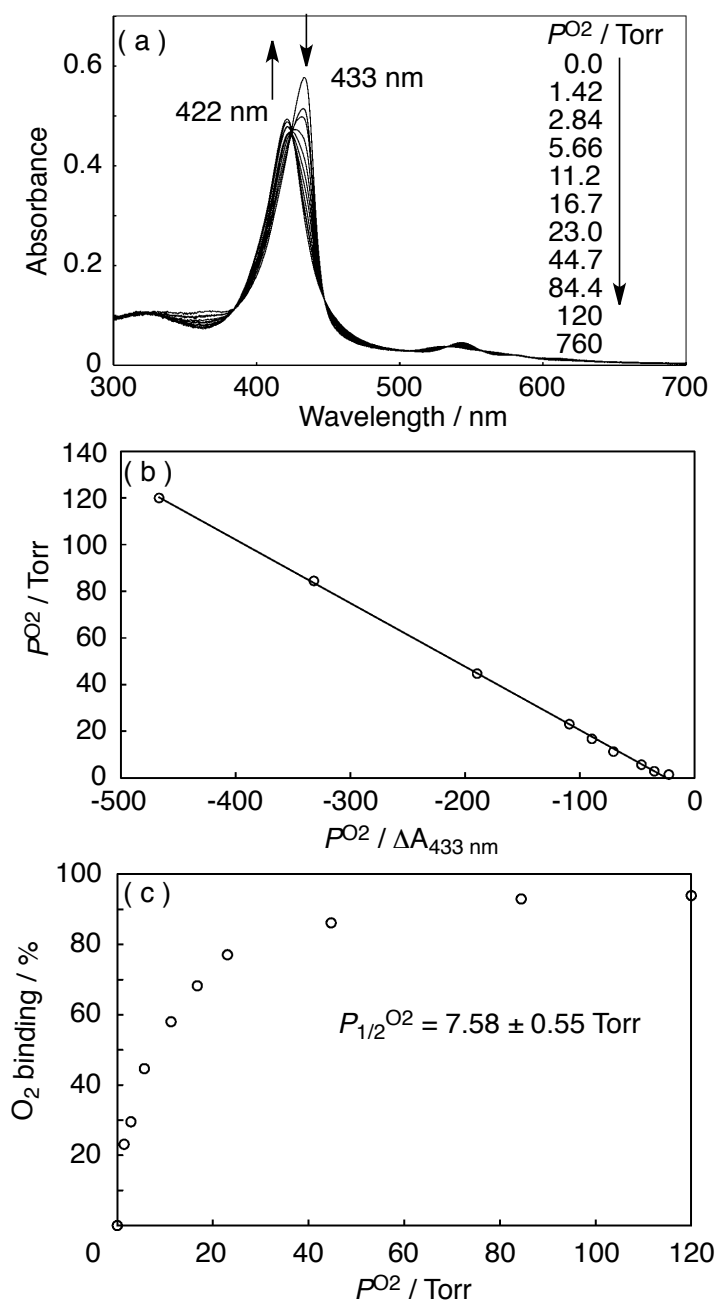


**Fig. S16** UV-Vis spectral changes of PEG20k-hemoCD (5.0 x 10<sup>-6</sup> M) as a function of the O<sub>2</sub> partial pressure ( $P^{O_2}$ ) in N<sub>2</sub> in 0.05 M phosphate buffer at pH 7.0 and 25 °C (a), plot of  $P^{O_2} / \Delta A_{433 \text{ nm}}$  versus  $P^{O_2}$  for determining  $P_{1/2}^{O_2}$  (b) and the titration curve for O<sub>2</sub> binding to PEG20k-hemoCD (c).

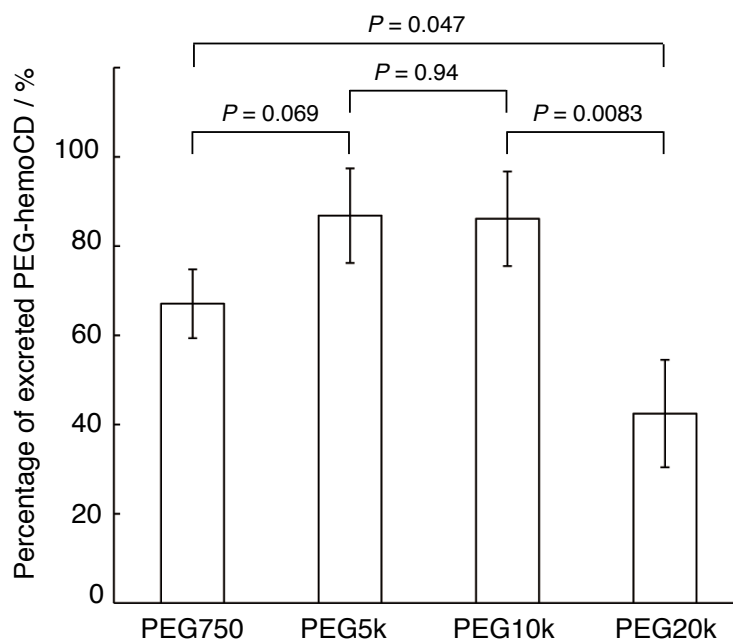


**Fig. S17** The amount of urinary excreted PEG(mw)-hemoCD at 6 h after the infusion of oxy-PEG(mw)-hemoCD ( $5 \times 10^{-4}$  M solution in PBS was infused to the femoral vein of a rat at the rate of 1.0 mL/h for 2 h). The *P* values obtained from student's T-test indicate the probability that the observed differences between the groups has occurred by chance.